Quantitative microstructural investigation of neutron-irradiated RAFM steel for nuclear fusion applications

O. J. Weiß, E. Gaganidze, J. Aktaa

Karlsruhe Institute of Technology, Institute for Materials Research II,

Hermann-von-Helmholtz-Platz 1, 76344 Eggenstein-Leopoldshafen, Germany

Abstract Reduced Activation Ferritic/Martensitic (RAFM) 7-10%Cr-WVTa steels are considered as primary candidate structural materials for in-vessel components of future fusion power plants. These components will be exposed to high neutron and thermo-mechanical loads. Accumulated neutron displacement damage along with transmutation helium generated in the structure materials due to 14.1 MeV fusion neutrons strongly influences the mechanical behavior of the materials. The intention of this work is to evaluate the microstructure of the neutron-irradiated RAFM steel EUROFER97. For this purpose irradiation induced defects like point defect clusters and dislocation loops were identified by transmission electron microscopy (TEM) and quantified in size and volume density. Long term objective is analyzing the influence of the irradiation dose and different neutron fluxes on the evolution of size and density of the defects at irradiation temperature of 300-330 °C.

EUROFER97 samples irradiated to 31.8 dpa were analyzed by TEM. The irradiation was carried out with a flux of 1.8×10^{19} $m^{-2}s^{-1}$ (> 0.1 MeV) in the BOR 60 fast reactor at Joint Stock Company (JSC) "State Scientific Centre Research Institute of Atomic Reactors" (SSC RIAR) in Dimitrovgrad, within the framework of the irradiation program "Associated Reactor Irradiation in BOR 60", which is named ARBOR-1 (Latin for tree).

The quantitative data obtained will be used to correlate the changes in the microstructure to the observed irradiation induced hardening and embrittlement of the material and will serve as an input for models describing this correlation.

T. Böllinghaus et al. (eds.), *Materials Challenges and Testing for Supply of Energy and Resources*, DOI 10.1007/978-3-642-23348-7_2, © Springer-Verlag Berlin Heidelberg 2012

1 Introduction

Since fuels are abundant and there is very restricted carbon emission, Nuclear Fusion is a clean way to supply our increasing energy demand. To achieve a fusion reaction the fuel consisting of Deuterium (D) and Tritium (T) – two isotopes of the light element Hydrogen (H) must be heated up to 100 Million degree Celsius. At these extreme temperatures the electrons are separated from the nuclei and the fuel becomes a plasma, which is confined in a magnetic field. Due to thermal energy, the velocity of the ions inside the plasma is high enough to overcome the natural electrostatic repulsion between positively charged atomic nuclei. Thus, when close enough, D-T are fused to heavier Helium (He) atoms, releasing a fast neutron and a total energy of 17.6 MeV per reaction. The uncharged neutrons are not affected by the magnetic field and can leave the plasma to the First Wall/Blanket of the reactor vessel, transferring their energy (14.1 MeV) as heat. In future fusion power plants this heat will be used to produce steam and thereby electricity.

One promising concept of magnetic confinement is the Tokamak with a doughnut-shaped vacuum vessel. This principle is used for the International Thermonuclear Experimental Reactor (ITER) which is currently being built in Cadarache/France [1]. Fig. 1 shows a cut-away view of the ITER Vacuum Vessel showing First Wall/Blanket modules and the Divertor at the bottom. In ITER various types of Test Blanket Modules will be installed. In a later demonstration reactor (DEMO) Breeding Blankets will be used to capture the neutrons, converting their energy to heat. They also allow for neutron multiplication and breeding of Tritium fuel.

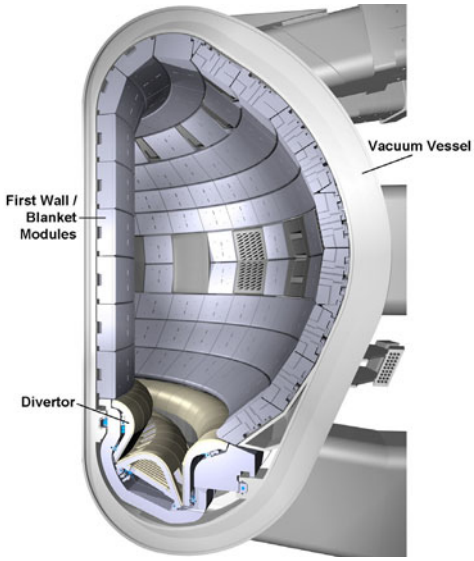

Fig. 1. A cut-away view of the ITER Vacuum Vessel showing the Blanket modules attached to its inner wall and the Divertor at the bottom (taken from www.iter.org).

Function of the Divertor is to pump away He ash and other impurities to maintain a high quality plasma. It consists of cooled structural material (heat sink) and plasma-facing material supported by the former.

Reduced Activation Ferritic/Martensitic (RAMF) steels e.g. EUROFER97 are primary candidate structural materials for the mentioned in-vessel components of future fusion power plants. Their chemical composition is based on the low activation elements Fe, Cr, W, V, Ti, Ta and C. In a fusion reactor the materials will be exposed to high neutron and thermo-mechanical loads. When hitting the material, high-energy neutrons create atomic displacement cascades, and besides a considerable amount of helium is generated by transmutation. The displacement damage accumulates during reactor operation and defects like point-defect clusters and dislocation loops are created. Together with He-bubbles and radiation induced precipitates these defects lead to strong low temperature hardening and embrittlement of the material [2]. Both effects are displayed in Fig. 2 a) and b), respectively.

Aim of this work is to quantify the influence of neutron irradiation on the microstructure of RAFM steels. Since no intensive irradiation facility with a fusion-like neutron spectrum exists, steel samples were irradiated under fission conditions to simulate fusion neutron damage. The samples were then investigated by transmission electron microscopy (TEM). Emphasis is put on measuring the sizes and volume densities of the irradiation-induced defects. These irradiation induced changes in the microstructure should be correlated to changes in mechanical material properties to identify dominant hardening/embrittlement mechanisms in RAFM steels.

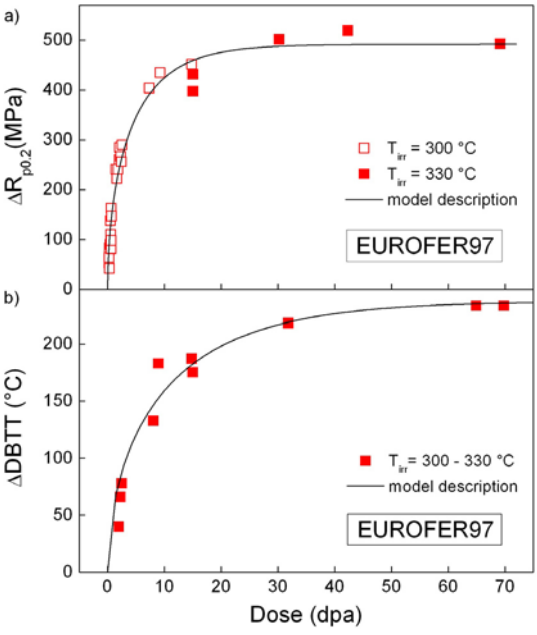

Fig. 2. a) Hardening of EUROFER97: the tensile stress increased with irradiation dose and saturated at about 20 dpa. b) Embrittlement led to an increase of the ductile-to-brittle transition temperature (DBTT) with irradiation dose. The DBTT shift saturated at much higher doses around 60 dpa, indicating the presence of non-hardening embrittlement mechanisms at high doses (from [2]).

2 Experimental

EUROFER97 charpy specimens with the composition 8.91Cr 1.08W 0.48Mn 0.2V 0.14Ta 0.006Ti 0.12C (wt-%, Fe balance) were irradiated to a dose of 31.8 dpa in the BOR 60 fast reactor at Joint Stock Company (JSC) "State Scientific Centre Research Institute of Atomic Reactors" (SSC RIAR) in Dimitrovgrad, within the framework of the irradiation program "Associated Reactor Irradiation in BOR 60", which is named ARBOR-1 (Latin for tree) [3]. The irradiation temperature was 332 °C and the neutron flux $1.8x10^{19}$ $m^{-2}s^{-1}$ (>0.1 MeV).

The specimens were impact-tested in the material science laboratory of RIAR and thereafter transported to the Fusion Material Laboratory (FML) of Karlsruhe Institute of Technology (KIT). From undeformed ends of the Charpy specimen tested at 138°C slices of 150 µm thickness were cut-off using a cutting wheel. The slices were then thinned by electrolytic polishing in a solution of 20% H_2SO_4 + 80% CH_3OH at room temperature with a Tenupol-5 jet polisher. In order to minimize radioactivity and magnetism, discs of 1 mm diameter including the electron-transparent region were punched out and put in foldable copper nets for examination in the TEM. Modification of the microstructure due to the 1 mm disc punching was not observed.

The TEM investigations were performed at 200 kV using a FEI Tecnai G2 F20 microscope equipped with a post-column GIF Tridiem energy filter (GATAN). The weak-beam dark-field (WBDF) technique [4] was used. To improve the contrast and remove contributions of inelastically scattered electrons in thicker regions of the sample, all images were zero-loss filtered with an energy slit of 15 eV. The diffraction conditions g(7.1g) for g={110} and g(4.1g) for g={200} were chosen, resulting in a diffraction error s_g of approximately 0.2 nm^{-1}.

3 Results

The martensitic microstructure of EUROFER97 irradiated to 32 dpa is shown in Fig. 3 a). Precipitates were located mainly at lath boundaries. Inside the grains the density of defects seems to be quite high. At a higher magnification dislocation loops could be clearly resolved as can be seen in the detailed picture Fig. 3 b). However, due to the bright-field dynamical diffraction condition the image peaks of the defects were very broad giving a complex contrast.

For quantitative analysis weak-beam dark-field imaging was used. The images were thereby confined to the physical sizes of the defects and narrow peaks allowed imaging of small defects down to 1 nm. For the investigation two different grains were chosen. They were tilted to g(7.1g) and g(4.1g) using diffraction vectors of the g={110} and g={200} type, respectively. Two resulting micrographs of

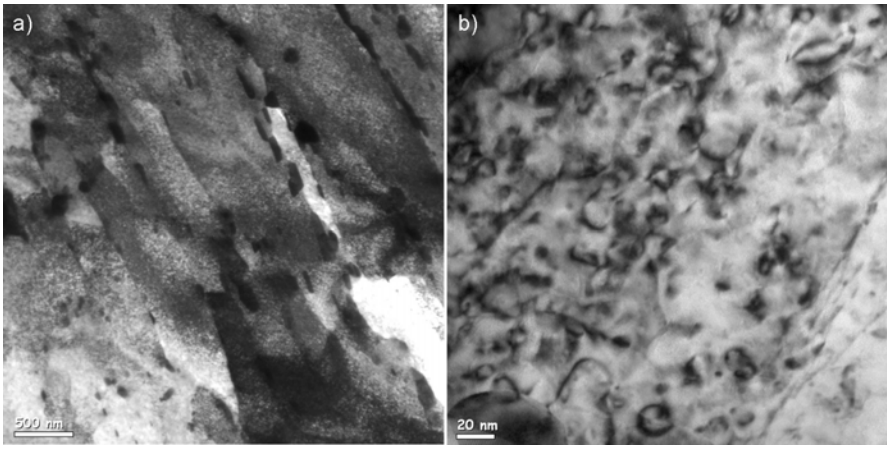

Fig. 3. a) Bright-field image of EUROFER97 irradiated to 32 dpa at 332°C showing the martensitic lath structure. Most of the grain boundaries are decorated with large precipitates. b) Defect microstructure at higher magnification showing dislocation loops and line dislocations.

grain #1 with g={110} are shown in Fig. 4 a) and b). Dislocation loops with diameters of up to 20 nm can be seen, as well as small defect clusters which are visible as white dots and thought to be of interstitial type. The loops generally appear edge on with a strong double arc contrast. To some extend the defects are hard to identify. This is on the one hand because it is not clear whether some white dots are actually small point defect clusters or belong to one of the arcs of larger dislocation loops. On the other hand the identification of the defect is hindered by the detrimental background contrast, which probably stems from surface contamination.

Fig. 4 c) and d) show micrographs of grain #2 with g={200}. Here the background contrast is less pronounced. It appears that most loops are aligned along {211} planes, which is common for bcc systems [6].

After image calibration the defects were marked manually with the line selection tool of the public domain software ImageJ [7]. Counting and sizing were done automatically with the built-in script functions. By this means an area of 1.72 μm² was analyzed. To get the volume density of the defects the foil thickness was measured by convergent beam electron diffraction (CBED) according to Kelly and Allen [8, 9]. For this purpose both investigated grains were tilted to different dynamical two-beam conditions. The recorded CBED patterns were analyzed using a DM-script by V. Hou [10] resulting in average thickness values of 146 nm and 106 nm for grain #1 and #2, respectively. The intensity profile of a {200} diffraction disc is exemplarily shown in Fig. 5.

The size distributions of defect clusters and dislocation loops are given in Fig. 6 a) and b) for grain #1 and #2, respectively. For the shown distributions more than 3600 defects were measured. The maximum loop diameter was 25 nm, while the

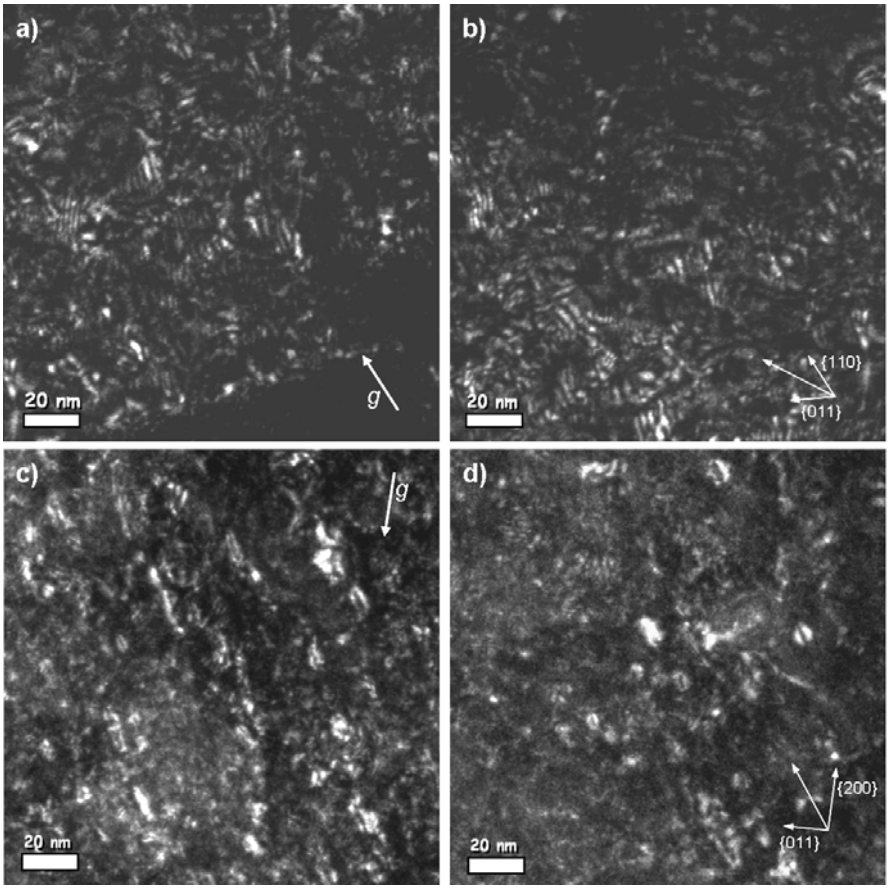

Fig. 4. a) and b) WBDF micrographs of grain #1 with g(7.1g), g={110} near a <111> zone axis; c) and d) WBDF micrographs of grain #2 with g(4.1g), g={200} near a <011> ZA. Most dislocation loops appear edge on with strong double arc contrast and diameters of up to 20 nm (taken from [5]).

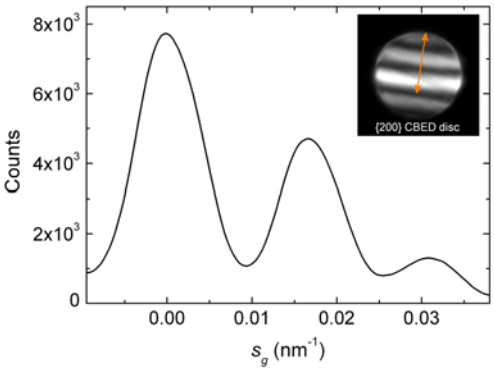

Fig. 5. Image of a {200} CBED disc near a <011> zone axis (inset) and the corresponding intensity profile used for thickness determination (taken from [5]).

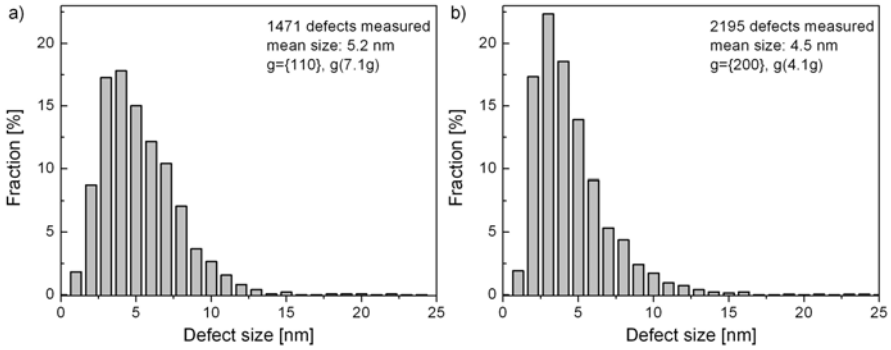

Fig. 6. Size distributions of radiation induced defects in EUROFER97 irradiated to 32 dpa at 332°C. a) Grain #1, the volume density is $1.4x10^{22}$ m^{-3} b) Grain #2, the volume density is $2.1x10^{22}$ m^{-3} (taken from [5]).

average value was about 5 nm for both cases. The defect densities were determined to $1.4x10^{22}$ m^{-3} and $2.1x10^{22}$ m^{-3}, respectively. To the best of our knowledge quantitative microstructural data of irradiated EUROFER97 was reported only once so far [11]. Similarly to our results, loops with sizes between 5 and 25 nm were detected after irradiation to 16.3 dpa. However, the defect density was about one order of magnitude lower than we measured, mainly because only defects clearly resolvable as dislocation loops were counted [12]. As listed in Table 1, investigations on F82H yielded densities similar to ours already at considerably lower irradiation doses of around 9 dpa. Concerning the dose-dependency it was shown that the defect density first increased with the dose up to a dose between 2.5 and 8.8 dpa and then decreased above [13], which might explain the relatively low defect density in EUROFER97 at 32 dpa. Nevertheless different metallurgical variables like the chemical composition, heat treatments and microstructure of EUROFER97 and F82H might influence defect accumulation during irradiation leading to different defect densities. Furthermore, it is important to notice that due to different orientations with respect to the direction of the electron beam only a fraction of loops is visible in the analyzed micrographs. To get more information about the fraction of invisible loops a section of the sample was imaged using three different diffraction vectors. The resulting micrographs are shown in Fig. 7.

Table 1. Comparison of quantitative microstructural data from different irradiated RAFM steels. Only neutron irradiation with an irradiation temperature T_{irr} in the range of 300-330°C was taken into account (taken from [5]).

Material	Irradiation source	Dose (dpa)	T_{irr} (°C)	Average defect size (nm)	Average defect density (m^{-3})	Reference
EUROFER97	n (BOR60)	31.8	332	4.9	1.75×10^{22}	This work
EUROFER97	n (HFR)	16.3	300	5-25	4.00×10^{21}	[11]
F82H	n (HFR)	8.8	302	5.4	4.50×10^{22}	[13]
F82H	n (HFR)	9.2	310	6.9	2.80×10^{22}	[13]

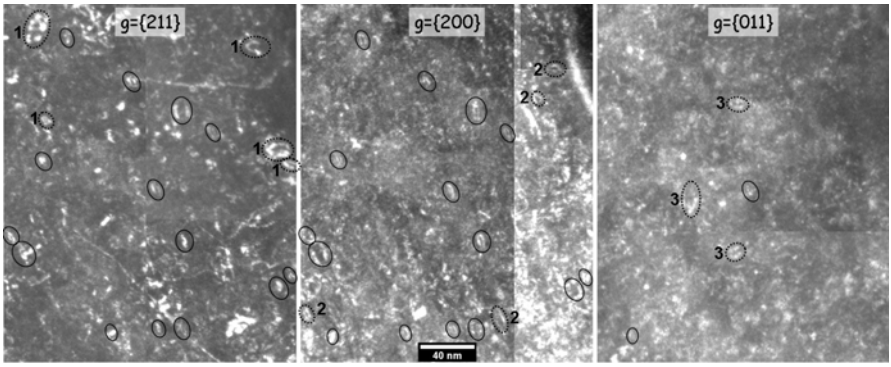

Fig. 7. A section of grain #2 imaged with 3 different diffraction vectors. The defect contrast changes due to different loop inclination after tilting the sample to the next diffraction condition. Loops visible in several images are marked with solid circles. Loops visible in only one of the micrographs are numbered 1-3 and marked with dashed circles. The stripes in the images stem from putting several micrographs together to get exactly the same sample section for each diffraction condition.

Comparing the images it is apparent that the contrast of the defects changed due to different loop inclination after tilting the sample to the next diffraction condition. Most of the loops – marked with closed circles – were visible using the g={211} and g={200} diffraction vectors (partially also with g={011}). Other loops – numbered 1-3 and marked with dashed circles – were only visible in one of the micrographs. To determine the Burgers vectors of the dislocation loops the invisibility criterion g·b=0 was used. Since the diffraction vectors were not exactly known, there is some ambiguity concerning the determination. Tables with all possible g·b combinations were hence used to identify the most probable Burgers vectors: b = <100> in case of the loops marked with '1' and b = ½<111> in all other cases. According to the three micrographs in Fig. 7 roughly 70% of the defects are visible in case of g={211} and g={200} and 19% in case of g={011}. These values are not very reliable, because only a very small area of the sample has been analyzed by this means so far. A systematic comparison of images taken from a much larger area is needed to reliably determine the ratio of loops with <100> and ½<111> type Burgers vectors. However, due to invisibility of defects the overall defect densities could be considerably higher than the reported values. Compared to the irradiation experiments listed in Table 1 the average loop size seems to be rather small for a high-dose irradiation of 32 dpa. Possibly in this case the irradiation temperature was just below the threshold for loop coarsening, which is believed to lie in the range of 330°C [13]. The size distribution of defects could be affected by two points: First, in some cases it was not possible to identify large loops unambiguously because of complicated diffraction and background contrast. Also white dot contrast of the arcs of some larger loops could have been misleadingly counted as small clusters leading to an underestimation of size and density of large loops.

4 Summary and Outlook

The microstructure of EUROFER97 neutron-irradiated to a high-dose of 31.8 dpa was analyzed quantitatively by means of WBDF microscopy. Irradiation induced defects like small point defect clusters and dislocation loops sized between 1 nm and 25 nm have been detected. The average size was 4.9 nm. The average volume density of visible defects was 1.75×10^{22} m^{-3}.

In a subsequent step the results will be compared to quantitative data from samples irradiated to a dose of 15 dpa. The systematic comparison of defects imaged with different diffraction vectors will be extended to larger areas which will allow drawing conclusions about the overall density of defects. The obtained quantitative data will be used to verify the ability of existing physical models for damage cascades to describe the evolution of the density and size of radiation-induced defects with irradiation dose. Our goal is to use the data as an input to model irradiation-induced hardening and embrittlement of EUROFER97.

Acknowledgements This work, supported by the European Communities under the contract of Association between EURATOM and Karlsruhe Institute of Technology (KIT), was carried out within the framework of the European Fusion Development Agreement. The views and opinions expressed herein do not necessarily reflect those of the European Commission. This work was also partly funded by Helmholtz Gemeinschaft e.V. under the grant HRJRG-013.

1 Ikeda, K.: ITER on the road to fusion energy. Nucl. Fusion **50**, 014002 (2010)
2 Gaganidze, E., Schneider, H.-C., Petersen, C., Aktaa, J., Povstyanko, A., Prokhorov, V., Lindau, R., Materna-Morris, E., Möslang, A., Diegele, E., Lässer, R., van der Schaaf, B., Lucon, E.: Mechanical Properties of Reduced Activation Ferritic/Martensitic Steels after High Dose Neutron Irradiation. Proc. of 22nd IAEA Fusion Energy Conference, 13-18 October 2008 Geneva, Switzerland; Paper FT/P2-1
3 Petersen, C., Shamardin, V., Fedoseev, A., Shimansky, G., Efimov, V., Rensman, J.: The ARBOR irradiation project. J. Nucl. Mater. **307-311**, 1655 (2002)
4 Cockayne, D. J. H., Ray, I. L. F., Whelan, M. J.: Investigations of dislocation strain fields using weak beams. Phil. Mag. **20**, 1265 (1969)
5 Weiß, O. J., Gaganidze, E., Aktaa, J.: Quantitative TEM investigations on EUROFER 97 irradiated up to 32 dpa. Submitted to Adv. Sci. Technol., Proceedings of the CIMTEC 2010
6 Byun, T., Hashimoto, N., Farrell, K., Lee, E.: Characteristics of microscopic strain localization in irradiated 316 stainless steels and pure vanadium. J. Nucl. Mater. **349**, 251(2006)
7 ImageJ, Image Processing and Analysis in Java. http://rsbweb.nih.gov/ij/
8 Kelly, P. M., Jostsons, A., Blake, R.. G., Napier, J. G.: The determination of foil thickness by scanning transmission electron microscopy. Phys. Stat. Sol. (a) **31**, 771 (1975)
9 Allen, S. M.: Foil thickness measurements from convergent-beam diffraction patterns. Phil. Mag. A **43**, 325 (1981)
10 Hou, V.: Thickness by CBED. Digital Micrograph(tm) Script Database, http://www.felmi-zfe.tugraz.at/dm_scripts/. Acessed 21 July 2010

11 Klimenkov, M., Materna-Morris, E., Möslang, A.: Characterization of radiation induced defects in EUROFER after neutron irradiation. Submitted to J. Nucl. Mater., Proceedings of the ICFRM-14, Sapporo (2009)
12 Klimenkov, M.: Private communication (2011)
13 Schäublin, R., Victoria, M., Lucas, G., Snead, L., Kirk Jr., M., Elliman, R. (ed.): Identification of Defects In Ferritic/Martensitic Steels Induced by Low Dose Irradiation. MRS Symp. Proc. **650**, R181 (2001)

http://www.springer.com/978-3-642-23347-0

Materials Challenges and Testing for Supply of Energy and Resources

Boellinghaus, Th.; Lexow, J.; Kishi, T.; Kitagawa, M. (Eds.)
2012, VIII, 296 p., Hardcover
ISBN: 978-3-642-23347-0